THE EUROPEAN
PHYSICAL JOURNAL
SPECIAL TOPICS

Regular Article

Linear and nonlinear mechanical responses of cell monolayers under crowding

Qing-Ling Guan[1,2], Li-Quan Dong[1,2,a], and Qun Hao[1]

[1] Beijing Inst Technol, Sch Opt & Photon, Beijing Key Lab Precis Optoelect Measurement Inst, Beijing 100081, People's Republic of China
[2] Beijing Inst Technol, Yangtze Delta Reg Acad, Jiaxing 314019, People's Republic of China

Abstract Epithelial monolayers play an important role in a broad range of physiological and pathological processes, such as embryonic development and wound healing. Epithelial monolayers become crowded during cell proliferation and growth, however, their mechanical properties entities remain obscure. This paper presents a novel and efficient method utilizing the structural stiffness matrix-based computational method (SMM) to investigate the mechanical characteristics of an epithelial monolayer as it undergoes varying degrees of crowding. Both D1-type extrusion, representing the extrusion of live cells, and D2-type extrusion, describing the extrusion of apoptotic cells, are examined. Our simulations reveal that the epithelial monolayer exhibits linear elastic behavior under slight crowding and nonlinear elastic behavior in response to overcrowding. These mechanical properties are significantly influenced by the strength of cellular cytoskeleton and the mode of cell extrusion. Moreover, our analysis indicates that the linear deformation of these monolayers is predominantly born by the variation in cell orientation, while the nonlinear deformation originates from the existence of the microtubules. This study further deepens our understanding of the relationship between the mechanical properties of cytoskeleton, individual cells and their monolayers, and may shed light on linking cell behavior to the patterning and morphogenesis of tissues.

1 Introduction

The epithelial monolayer plays an important role in a broad range of physiological and pathological functions, such as morphological changes in embryonic development [1], protective barrier on surfaces of organs [2] and collective cell migration in wound healing [3]. These indispensable functions require the tight association of its constituent cells by the adhesion junctions that mechanically stabilize the tissue [4–6]. Many developmental defects or clinical pathologies in the form of impaired cell–cell associations will occur when cells are unable to withstand mechanical stimuli due to gene mutations or pathological disturbances [7, 8]. In light of this, it becomes apparent that the quest to apprehend the mechanical intricacies of epithelial morphogenesis is a formidable task that holds immense significance in developmental biology.

Owing to the acknowledgment of its critical role in biological functions, growing attention has been paid to investigating the morphologies and properties of epithelia in varying mechanical environments [9–12].

Numerous captivating and substantial physical phenomena have been documented in the analysis of these experimental investigations. Serra-Picamal et al. [9, 10] experimentally reported the identification of an X-type mechanical wave that propagates slowly throughout the monolayer during the free expansion of cell monolayers. Their investigation also revealed that this wave is regulated by myosin protein activity, cell–cell interactions, and cytoskeletal remodeling. Brugues et al. [3] discovered patterns of traction forces pointing toward the wound by quantifying the map of traction force in an epithelial monolayer. Harris et al. [13, 14] proposed a device to measure the mechanical properties of the stretched monolayers, and revealed that the strength and stiffness of epithelial monolayers are contingent upon the topology of their constituent cells and the tight junctions between adjacent cells. Recently, Eisenhoffer et al. [15] and Marinari et al. [16] independently delineated the phenomenon of epithelial overcrowding, which may engender the extrusion of viable cells as well as cell death. Subsequently, Liu et al. [17] conducted simulations that validated the capacity of both these

2718

Eur. Phys. J. Spec. Top. (2023) 232:2717–2725

forms of cell extrusion to preserve the homeostatic density of cells and an optimal stress threshold of the monolayer under conditions of overcrowding. Nevertheless, despite these insightful findings, the mechanical underpinnings of dense epithelial tissues that arise from cell proliferation and migration continue to pose a significant enigma in the realm of developmental biology.

The mechanical characteristics of compact tissue are typically governed by three fundamental properties at the cellular level: the ability of individual cells to migrate, the persistence of cell migration, and a target cell shape index [18]. These factors and their effect on tissue mechanical states have been thoroughly investigated and explained in the literature [19–21]. One specific factor, namely the effect of cytoskeletal mechanical stiffness within dense tissues, has largely been overlooked in discussions concerning tissue mechanics. It is widely recognized that cell death processes are highly mechanosensitive and heavily reliant on various crucial cellular parameters, such as local cell density, cell shape, interface area between cells, intra-cellular tension, and paracrine biochemical signaling [22–25]. Many of these cellular parameters are strongly correlated with cytoskeletal strength [26, 27]. Therefore, neglecting the mechanosensitive pathways that lead to cellular death while elucidating tissue mechanics, specifically during significant biological events such as embryogenesis, wound healing, and cancer progression, can significantly constrain our comprehension of these complex processes.

Several theoretical and computational techniques have been developed for simulating cell behavior within the epithelial monolayer, including the Cellular Potts model, Flocking model, Phase-field model, and Vertex model [28–31]. However, despite the promise of simulating large-scale tissues, most existing models lack consideration for detailed cytoskeletal structures, and incur high computational costs. Recently, Yin et al. [32] proposed a computational method based on a structural stiffness matrix (SMM) that provides an efficient tool for accurately and rapidly evaluating the mechanical properties of cell monolayers. Importantly, this approach naturally incorporates the structural features of cells, which are often neglected in other methods. In this paper, we employ this modeling framework to investigate the mechanics of epithelial monolayer under variable extents of crowding characterized by distinct compression strains. D1- and D2-type cell extrusions are chosen to express the extrusion of live cells and cell death, respectively. Our findings suggest that the monolayer exhibits linear elastic and nonlinear elastic behaviors in different compression stages. The linear deformation of the monolayer arises from cell orientation transition, while the nonlinear deformation originated from the resistance of the cytoskeleton. Moreover, the cytoskeletal strength changes, including adhesive strength, contraction and microtubule stiffness, and the modes of cell extrusion, are found to significantly affect the mechanical properties of the crowded monolayer.

2 Methods

In this investigation, we utilize the SMM method [32] to examine collective cell behavior in response to a variable crowded environment. The approach involves describing the monolayer as a sequence of polygons, each representing a cell, which was then modeled as a tensegrity structure [33–36]. The cell membrane is depicted as a series of strings capable of bearing solely tensile forces, while the internal microtubules were represented as a suite of bars able to resist both compressive and tensile forces [37–39], as illustrated in Fig. 1a, b. Within this framework, cell position and shape changes are expressed through the motions of vertices and nucleus.

We first derive the force vector and structural stiffness matrix of an individual cell, designated by α. The α - th cell packing geometry is described by N_α^{v} vertices including 1 nucleus and $N_\alpha^{\mathrm{v}}-1$ membranal vertices, and N_α^{e} elements including N_α^{m} microtubule elements and N_α^{s} membranal elements. The total mechanical energy of the α-th cell is composed of the contributions of the area elastic energy of the cell V_α^{v}, the adhesion energy V_α^{a}, the contraction energy V_α^{c}, and the microtubules deformation energy V_α^{m}, and is formally expressed as:

$$
\begin{aligned}
V_\alpha &= V_\alpha^{\mathrm{v}} + V_\alpha^{\mathrm{a}} + V_\alpha^{\mathrm{c}} + V_\alpha^{\mathrm{m}} = \frac{K}{2}(S_\alpha - S_0)^2 \\
&+ \sum_{e(ij)=1}^{N_\alpha \mathrm{s}} \Lambda l_{e(ij)} + \sum_{e(ij)=1}^{N_\alpha \mathrm{s}} \frac{\Gamma}{2} l_{e(ij)}^2 + \sum_{e(1j)=1}^{N_\alpha \mathrm{m}} \\
&\times \frac{B}{2}\left(l_{e(1j)} - l_0\right)^2,
\end{aligned}
\tag{1}
$$

where K, Λ, Γ and B represent the areal stiffness, interfacial tension, contraction modulus and microtubule stiffness, respectively; $l_{e(ij)}$ and $l_{e(1j)}$ indicate the current length of the membranal element $e(ij)$ interconnecting vertices i and j, as well as microtubule elements $e(1j)$ linking the nucleus 1 and vertex j, with i, $j = 2$, $\ldots$, N_α^{v}; l_0 and S_0 correspond to the preferred length of each microtubule and the preferred area of the cell.

With these energy forms, the forces exerted on the nucleus are comprised of microtubule force and random force. Each membranal vertex is subjected to adhesion force, contraction force, microtubule force, area-elastic force, and random force. Where, the first four terms are considered potential force and can be derived via the negative gradient of the potential energy V_α defined in Eq. (1) with respect to the coordinates of vertices $\mathbf{r}$, i.e. $\mathbf{F}_\alpha^{\mathrm{P}} = -\partial V/\partial \mathbf{r}$. Thus, the total force vector $\mathbf{F}_\alpha$ of the α-th cell can be determined via summation [41, 42]:

$$
\mathbf{F}_\alpha = \mathbf{F}_\alpha^{\mathrm{P}} + \mathbf{F}_\alpha^{\mathrm{R}} = \mathbf{F}_\alpha^{\mathrm{v}} + \mathbf{F}_\alpha^{\mathrm{a}} + \mathbf{F}_\alpha^{\mathrm{c}} + \mathbf{F}_\alpha^{\mathrm{m}} + \mathbf{F}_\alpha^{\mathrm{R}} \in \mathbf{R}^{2N_\alpha \mathrm{v}},
\tag{2}
$$

where $\mathbf{F}_\alpha^{\mathrm{v}}$, $\mathbf{F}_\alpha^{\mathrm{a}}$, $\mathbf{F}_\alpha^{\mathrm{c}}$, $\sqrt{S_0}$ and $\mathbf{F}_\alpha^{\mathrm{R}}$ represent area-elastic, adhesion, contraction, microtubule, and random force

Eur. Phys. J. Spec. Top. (2023) 232:2717–2725

2719

Fig. 1 Illustration of the model of cell monolayer containing cytoskeletal structures. (**a**) Immunostaining of Madin Darby canine kidney cell monolayer, where the green and blue colors represent actin cytoskeleton and nucleus, respectively [40]. (**b**) Shape description of cells, containing membrane, nucleus, and microtubules. (**c**) Cell intercalation. (**d**) Cell division. (**e**) D1-type cell extrusion. (**f**) D2-type cell extrusion
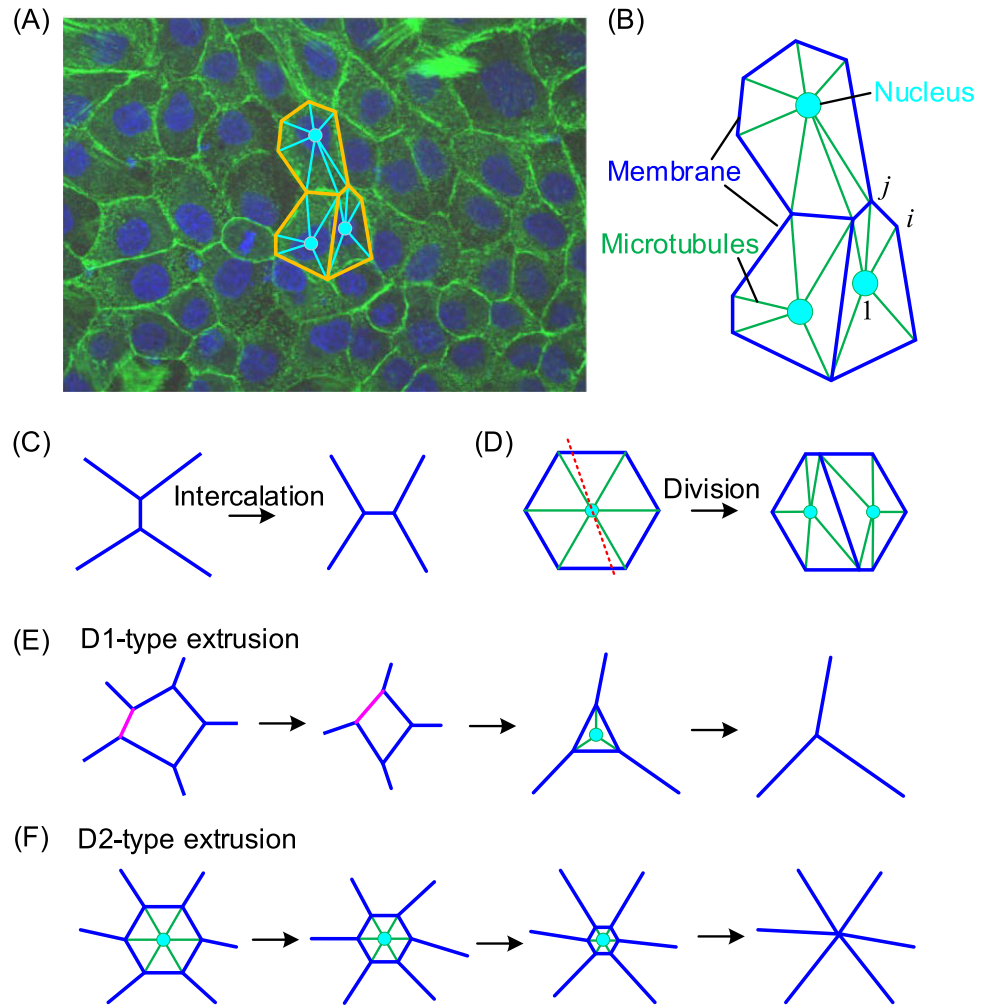
vectors, respectively. To account for stochastic fluctuations in the local microenvironment, the random force vector $\mathbf{F}_\alpha^R$ is incorporated into the simulations [43] and is formally defined as follows:

$$\langle F_{i,x}^R(t) F_{i,y}^R(t') \rangle = \gamma^2 \delta(t-t') \delta_{xy}, \qquad (3)$$

where t denotes time, γ represents the magnitude of the fluctuation, δ and δ_{xy} are Dirac's and Kronecker's δ-functions, respectively. The stiffness matrix of the α-th cell is then solved by taking the derivative of the potential force vector to the vertex coordinate vector, that is,

$$\mathbf{K}_\alpha = \frac{d\mathbf{F}_\alpha^P}{d\mathbf{r}} = \mathbf{K}_\alpha^v + \mathbf{K}_\alpha^a + \mathbf{K}_\alpha^c + \mathbf{K}_\alpha^m \in \mathbf{R}^{2N_\alpha v \times 2N_\alpha^v}. \qquad (4)$$

where $\mathbf{K}_\alpha^v$, $\mathbf{K}_\alpha^a$, $\mathbf{K}_\alpha^c$ and $\mathbf{K}_\alpha^m$ denote the matrices of area-elastic stiffness, adhesion stiffness, contraction stiffness and microtubule stiffness, respectively. Let the monolayer comprise N_c cells and N_v vertices, such that the sizes of the force vector and stiffness matrix of each cell can be expanded as $\hat{\mathbf{F}}_\alpha \in \mathbf{R}^{2N_v}$ and $\hat{\mathbf{K}}_\alpha \in \mathbf{R}^{2N_v \times 2N_v}$

respectively. The components of these matrices are embedded into the appropriate positions, following the global sequences. Then, the total force vector $\mathbf{F}$ and structural stiffness matrix $\mathbf{K}$ are obtained by simply summing the matrices of all the constituent cells:

$$\mathbf{F} = \sum_\alpha \hat{\mathbf{F}}_\alpha, \quad \mathbf{K} = \sum_\alpha \hat{\mathbf{K}}_\alpha. \qquad (5)$$

To ensure the positive definiteness of the stiffness matrix and avoid numerical divergence, $\mathbf{F}$ and $\mathbf{K}$ are modified as $\tilde{\mathbf{F}}$ and $\tilde{\mathbf{K}}$ [32]. The vertex displacements in each iteration step are then obtained:

$$^n\Delta\mathbf{r} = \left(^{n-1}\tilde{\mathbf{K}} \right)^{-1} \cdot {}^{n-1}\tilde{\mathbf{F}}, \qquad (6)$$

where n is the iteration step. The detailed derivations of the above formulas are given in [32].

The numerical simulations under consideration involve three distinct topological transitions that are employed to characterize the cellular biological processes in question. These transitions include cell intercalation, cell division, and cell extrusion, as clearly

2720

Eur. Phys. J. Spec. Top. (2023) 232:2717–2725

illustrated in Fig. 1c–f. The act of cell intercalation (Fig. 1c) refers to the exchange of cell neighbors, which is triggered when the distance between two vertices falls below a specified threshold value l_T. The topological transition process of cell division during tissue growth is displayed in Fig. 1d. This transition describes the phenomenon of a single cell dividing into two daughter cells, along a randomly oriented division axis that passes through the cell's geometric center. After the division process is complete, the nucleus of each daughter cell is relocated to its corresponding geometric center. Experimental findings suggest that the probability of cell division increases proportionally with the geometric size of the cell in question [44]. To characterize this biological behavior, the probability function of cell division is established [5]:

$$P_d = 1 - \exp\left(\frac{\Delta A_d - A_\alpha}{A_0}\right), \qquad (7)$$

where A_d is a parameter regulating the division probability. When the cell area exceeds A_d, the probability P_d is calculated and then the cell division occurs if a generated random number is less than P_d. Cell extrusion refers to the removal of a cell from a monolayer and is posited to transpire when the area of a cell descends below a designated threshold value A_E. Experiments showed that two types of cellular extrusion occur in response to overcrowding: D1- and D2-type cell extrusions [45]. The former describes the extrusion of live cells that accompanies a gradual loss of junctions, and occurs only when a triangular cell becomes smaller than a specified threshold. The latter represents the extrusion of apoptotic cells, in which the cells contract rapidly without experiencing junction loss and take place as the cellular area is below a threshold. The dynamic processes underlying these two types of cell extrusions are presented in Fig. 1e, f, respectively.

3 Results and discussion

In this study, the mechanical behaviors of the epithelial monolayer are assessed by the present SMM in response to different crowded environments. D1- and D2-type cell extrusion, representing the apoptosis-independent and dependent cell extrusions respectively, are both considered [15, 44]. Furthermore, the impacts of cellular cytoskeleton strength changes on the monolayer mechanics are investigated. For instance, 100 randomly distributed cells, depicted by Voronoi tessellations, are placed into a box with periodic boundaries. In the following simulations, the box size is fixed in the longitudinal direction (y-axis) and compressed in the lateral direction (x-axis) [13, 46]. For the sake of simplicity, yet without sacrificing generality, $\sqrt{A_0}$ and $KA_0^{3/2}$ are specified as unit length and unit force, respectively. Thereafter, other parameters can be readily normalized and assigned: $A_0 = 1$, $A_d = 1.3A_0$, $A_E = 0.1A_0$, $l_T = 0.05$,

$K = 1$, $\Gamma = 0.1$, $\Lambda = 0.1$, $B = 0.5$, and $\gamma = 0.02$. Unlike the simulations conducted by Liu et al. [17], our system is considered to reach stability and convergence when the relative difference between the energies of the system at two neighboring steps is less than 10^{-7}. In addition, we disregard the fluctuation of proteins aggregating along the cell surface.

To quantitatively evaluate the mechanical properties of the monolayer, some global mechanical parameters are defined: the number of cells extrusion N_e, the stress of the monolayer in the lateral direction σ_x and the longitudinal direction σ_y, mean cellular orientation H, and aspect ratio R. The strain and stress can be calculated using the following:

$$\varepsilon = \frac{L_x - L_0}{L_0}, \ \sigma_x = \frac{F_x}{L_y} = -\frac{\partial E}{L_y \partial x}, \ \sigma_y = \frac{F_y}{L_x} = -\frac{\partial E}{L_x \partial y}, \qquad (8)$$

where L_x and L_y denote the current lengths of monolayers along x-axis and y-axis directions, respectively; F_x and F_y are the corresponding forces acting on the monolayer in x-axis and y-axis directions, respectively. The mean cellular orientation H is specified to express their orientation distribution [5]

$$H = \langle \cos 2\theta \rangle, \qquad (9)$$

where θ refers to the cellular orientation and $\langle \cdots \rangle$ represents the average of all cellular orientations within the monolayer. On basis of this definition, $H = 0$ signifies that the cells within the monolayer are randomly orientated. $H = 1$ and $H = -1$ indicate the cells are oriented parallel and perpendicular to the compression direction, respectively. The aspect ratio R is defined as the ratio between the long and short axes of the ellipse that fits the cell shape.

3.1 Mechanical behaviors of monolayers in response to crowding

Experiments have shown that the elastic deformation of the monolayer plays a pivotal role in upholding its steady functionality in the face of external stimuli, particularly in crowded conditions [13, 47]. To simulate varying crowding extent, the epithelial monolayer is subjected to compressive loading via linear strain along the horizontal axis (x-axis). The deformation responses with D1- and D2-type cell extrusion are then calculated and depicted in Figs. 2 and 3, respectively. Its mechanical behaviors are described in terms of the variations in the number of extruded cells N_e, global stress of monolayer in the lateral direction σ_x and the longitudinal direction σ_y, mean cellular orientation H and aspect ratio R concerning the strain ε.

For D1-type extrusion (see Fig. 2), the deformation process of the monolayer can be divided into two regions: linear region and nonlinear. In the linear region (e.g. $\varepsilon = 0 \sim 30\%$), the stress σ_x and σ_y take a linear decrease with respect to compression strain ε_x,
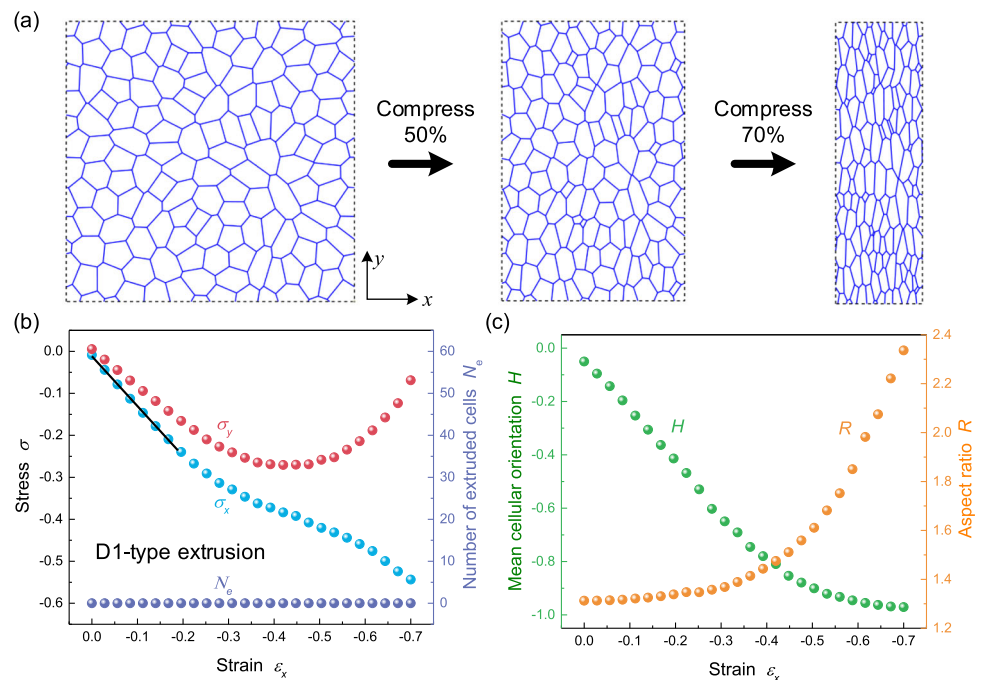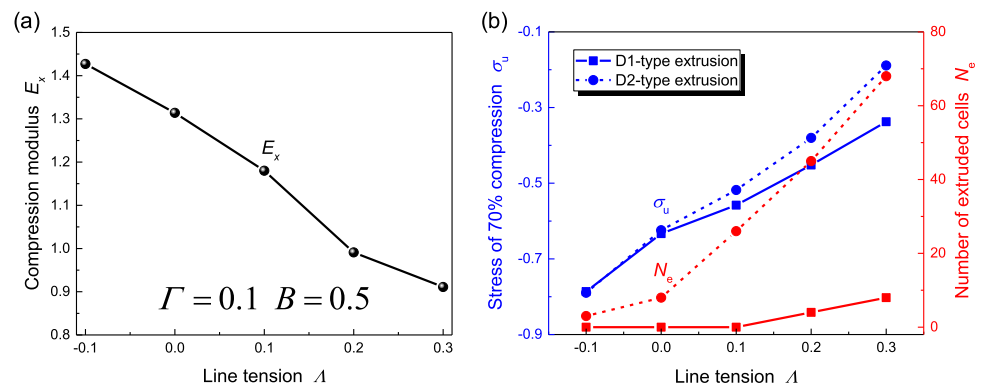
Fig. 2 Mechanical responses of monolayers with D1-type cell extrusion under linear strain compression. (**a**) Snapshots of cell configurations in the monolayer under different strain levels: $\varepsilon = 0\%$, -50% and -30%. Mechanical responses of monolayers are described by the variations of (**b**) number N_e of cell extrusion, stress in the lateral direction σ_x and the longitudinal direction σ_y, and (**c**) mean cellular orientation H and aspect ratio R with respect to the strain ε. The data are averaged over five simulations

Fig. 3 Mechanical responses of monolayers with D2-type cell extrusion under linear strain compression. (**a**) Snapshots of cell configurations in the monolayer under different strain levels: $\varepsilon = 0\%$, -50% and -30%. Mechanical responses of monolayers are described by the variations of (**b**) number N_e of cell extrusion, stress in the lateral direction σ_x and the longitudinal direction σ_y, and (**d**) mean cellular orientation H and aspect ratio R with respect to the strain ε_x. The data are averaged over five simulations
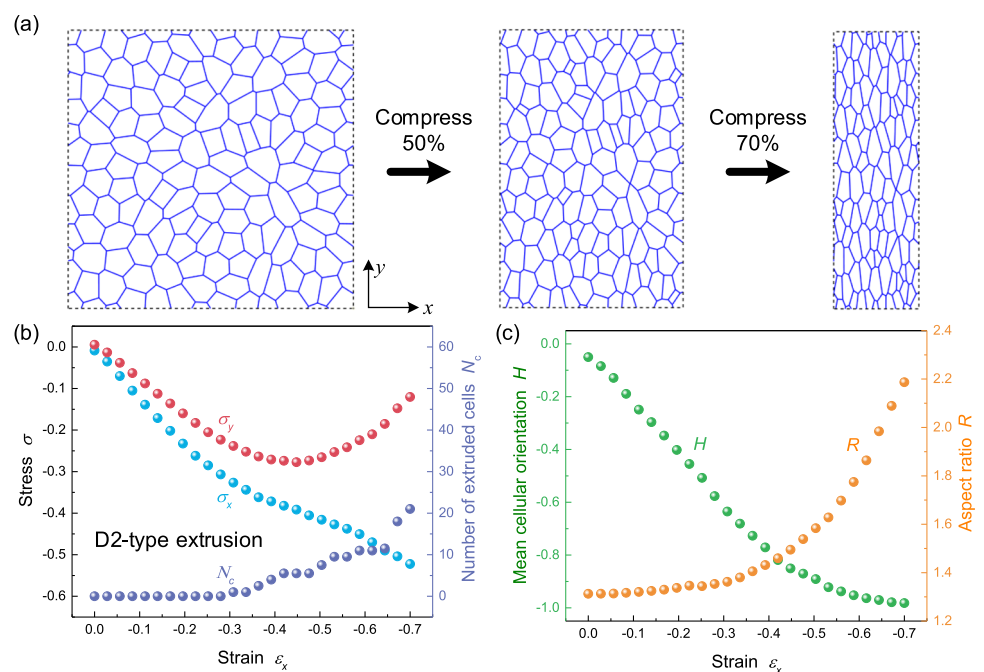
while the number of extruded cells remains constant, $N_e = 0$, as shown in Fig. 2b. The compression modulus E_x in x-axis direction can be calculated by fitting the stress–strain curve: $E_x = 1.18$. During this region, the mean cellular orientation H tends to reduce rapidly and linearly ($H = 0 \sim -0.65$), while the aspect ratio R presents slowly linearly increasing ($R = 1.32 \sim 1.41$), as illustrated in Fig. 2c. This indicates that the monolayer deformation at low-level compression strain is mainly the transformation of long axis orientation of cells. In the nonlinear region (e.g. $\varepsilon = 31 \sim 70\%$), the stress σ_x rises nonlinearly, σ_y goes down first and then up, while

the number N_e of extruded cells remains at 0. Meanwhile, H drops slowly from $H = -0.65$ to $H = -1$, while R increases quickly from $R = 1.41$ to $R = 2.38$, indicative of compression of the cell in the loading direction and gradual alignment toward the vertical direction of the loading. This result shows in this region that the applied compression is borne by mainly the geometric change of cellular shapes. Throughout the compression process, no extruded cell is observed in the monolayer, despite the existence of numerous small cells in the configuration (see Fig. 2a). This phenomenon could be attributed to the current cellular parameters being

2722

Eur. Phys. J. Spec. Top. (2023) 232:2717–2725

Fig. 4 Mechanical properties of crowded monolayers under various line tension levels. The variations of (**a**) compression modulus E_x, and (**b**) number of extruded cells N_e and stress σ_u in the x-axis direction at ending load with respect to interfacial tension Λ

unfavorable for cell intercalation, which subsequently affects the D1-type cell extrusion [17].

The mechanical properties of monolayers with D2-type extrusion exhibit a resemblance to those with D1-type extrusion (Fig. 3), while their difference is the nonlinear region. In this region, the number N_e of cell extrusion takes a growth trend with increasing strain ε_x. This variance from D1-type is primarily due to the non-dependence of D2-type cell extrusion on cell intercalation. The stress in the compression direction ($\sigma_x = -0.52$) at the ending load is larger than that of D1-type extrusion ($\sigma_x = -0.55$), while the longitudinal stress and the aspect ratio ($\sigma_y = -0.11$, $R = 2.21$) are less than that ($\sigma_y = -0.06$, $R = 2.35$), implying that cell extrusion can effectively dissipate the compression stress in monolayer, as observed in experiments [16, 17]. These findings indicate that in response to crowding, live cell extrusion acts a crucial role in maintaining the homeostatic cell density of the epithelial monolayer.

3.2 Mechanical properties of monolayers at different line tension levels

Experimental findings have revealed a significant correlation between the mechanics of monolayers and the cellular cytoskeleton, encompassing myosin, intercellular adhesions, and actin cytoskeleton [13]. To further investigate their respective roles, the influences of molecular and cellular perturbations on the mechanical properties of crowded monolayers are evaluated in the ensuing subsections. Our simulations have indicated that all responses can be classified into linear and nonlinear regions (data not presented) similar to Fig. 2b, c. To describe the mechanical features of the responses, three indices have been formulated, comprising the number of cell extrusion N_e, the compression modulus E_x fitted in the linear region, and the final stress σ_u in the x-axis direction at the ending load.

The mechanical properties of monolayers in response to crowding under various cellular adhesion strengths (expressed as line tension Λ) are first investigated, as depicted in Fig. 4. The obtained result reveals that an increase in line tension Λ leads to a decline in the compression modulus E_x (see Fig. 4a). For D1-type extrusions, the number N_e of extruded cells first

keeps zeros and then grows, and the stress σ_u increases monotonically (Fig. 4b). For D2-type extrusion, N_e and σ_u are both monotonically increasing. This trend is attributed to weaker cellular adhesion (indicated by a larger value of Λ), which preferentially produces a smaller cell perimeter, generates more cell extrusions during compression, and subsequently reduces the absolute value of final stress σ_x. Additionally, the shorter cell edge is able to produce more cell intercalation, resulting in more D1-type cell extrusion, consistent with experiments in that live cell undergoes a sequential loss of cell–cell junctions before extrusion [16].

3.3 Mechanical properties of monolayers at different molecular contraction levels and microtubule stiffness

In this subsection, we investigate thoroughly the dependence of mechanical properties of crowded monolayers on the contractility of actin-myosin rings and the rigidity of the microtubules. They are modeled by the parameters Γ and B respectively, which are both positive. A larger value of Γ and B will tend to suppress the geometric extension of cells.

For the microtubule stiffness and molecular contraction levels under study, the corresponding curves similar to Fig. 2a are gained, as depicted in Figs. 5 and 6. It can be seen that with the strengthening of contractile modulus K_c or microtubule stiffness K_m, the monolayers exhibit almost analogous mechanical variation patterns in response to crowding. For two extrusion types of cell, the compress modulus E_x and stress σ_u both take a monotonic increase. Their difference is that the number N_e of extruded cells keeps almost constant for both D1- and D2-type extrusion with increasing Γ, while N_e remains zero for D1-type extrusion and exhibits a growth trend for D2-type extrusion as growing B. The high contraction ability and microtubule stiffness favor the generation of an isotropic cell configuration at a constant area, and consequently, changes in their values do not affect the number of D1-type cell extrusions. However, higher microtubule stiffness can resist cell shrinkage in response to overcrowding, thereby leading to the extrusion of more D2-type cells to resist the anisotropic deformation of the monolayer.

Eur. Phys. J. Spec. Top. (2023) 232:2717–2725

2723

Fig. 5 Mechanical properties of crowded monolayers under various microtubule stiffnesses. The variations of (**a**) compression modulus E_x, and (**b**) number of extruded cells N_e and stress σ_u in the x-axis direction at ending load with respect to microtubule stiffness B
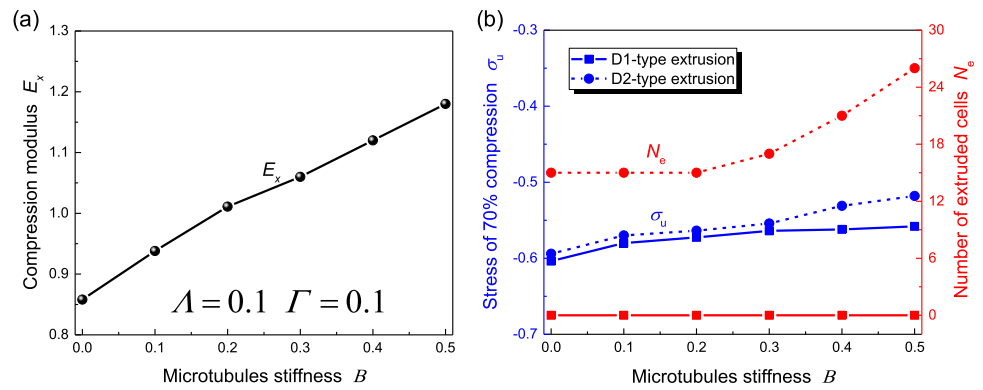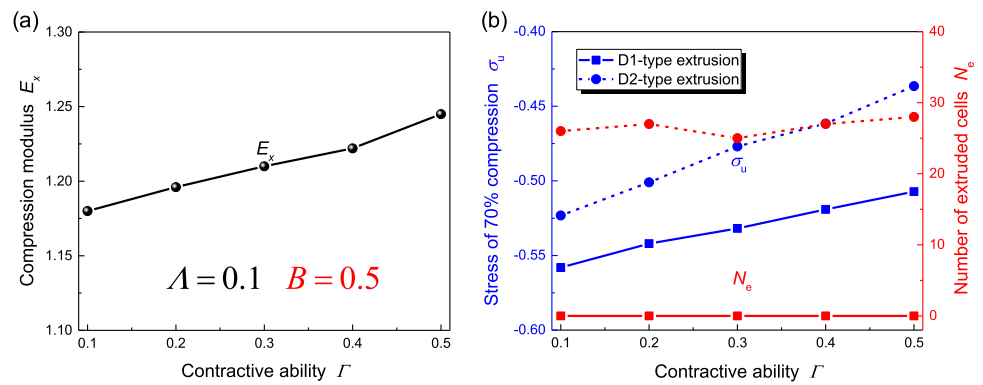

Fig. 6 Mechanical properties of crowded monolayers under various contractive modules. The variations of (**a**) compression modulus E_x, and (**b**) number of extruded cells N_e and stress σ_u in the x-axis direction at ending load with respect to contractive modulus Γ

It is also noteworthy that the variation in contractility has almost no effect on the number of D2-type cell extrusions, which is attributed to the presence of microtubules."

To further investigate the role of the cytoskeleton in monolayer mechanics, the mechanical responses of epithelial monolayers without cellular microtubules under compression are simulated in Fig. 7 and compared with that in Fig. 6. Unexpectedly, the elastic modulus E_x and stress σ_u of D1-type extrusion both drop monotonously with the increase of Γ for $B = 0$, while the number N_e of D2-type cell extrusion grows monotonously. Their variation trends are opposite in the case of $B = 0.5$. This is because the cell morphology is mainly determined by the actin-myosin ring when the microtubules are ignored. As the contractive modulus Γ grows, cells tend to shrink in size, inducing more D2-type cell extrusions. Meanwhile, the side length of a cell in the compression direction becomes shorter, resulting in a smaller tension σ_u for D1-type extrusion and a smaller compression modulue E_x. In addition, the mechanical process of a specific example with parameters $\Lambda = 0.1$, $\Gamma = 0.1$, $B = 0$ is described, as shown in Fig. 8. It is surprising to find that the stress σ_x in the x-axis direction of the cell monolayers without microtubules takes a linear drop during compression. The above variation is not affected by the form and number of extruded cells by comparing Fig. 8a, b. The stresses in the x-axis σ_x and y-axis direction σ_y in the nonlinear region are both less than those in the presence of the microtubules (compared with Figs. 2 and 3). These findings suggest that the cellular microtubules are beneficial in relieving the stress of cell monolayers in response to overcrowding. The above analysis indicates that the cytoskeleton plays an indispensable role in monolayer mechanics.

4 Conclusions

In summary, we studied the mechanical properties of crowded epithelial monolayers at different cytoskeletal strengths and cell extrusion types by using a structural stiffness matrix computational method. Our findings indicate that the deformation curves of monolayers exhibit both linear elastic and nonlinear elastic regions. The linear region in these monolayers is primarily governed by alterations in cell orientation, while the nonlinear deformation of monolayers is contributed by the presence of microtubules. The compression modulus of cell monolayers increases with the enhancement of the ability of actin-myosin rings to contract and the rigid of cell microtubules or with the reduction of the adhesion strength of E-cadherins. The stress of a crowded monolayer is relieved through cell extrusion and cytoskeleton remodeling. This study thus illuminates the mechanisms underlying the topological changes of cells in epithelia subjected to mechanical stimuli and has the potential to enhance our comprehension of the roles of sub-cell and cell mechanics in epithelial properties. It is worth mentioning that this computational method exhibits significant potential in simulating multi-scale behaviors of three-dimensional

2724

Eur. Phys. J. Spec. Top. (2023) 232:2717–2725

Fig. 7 Mechanical properties of crowded monolayers without cytoskeleton under various contractive abilities. The variations of (**a**) elastic modulus E_x, and (**b**) number of cell extrusion N_e and stress σ_u in the x-axis direction at ending load with respect to contractive ability Γ
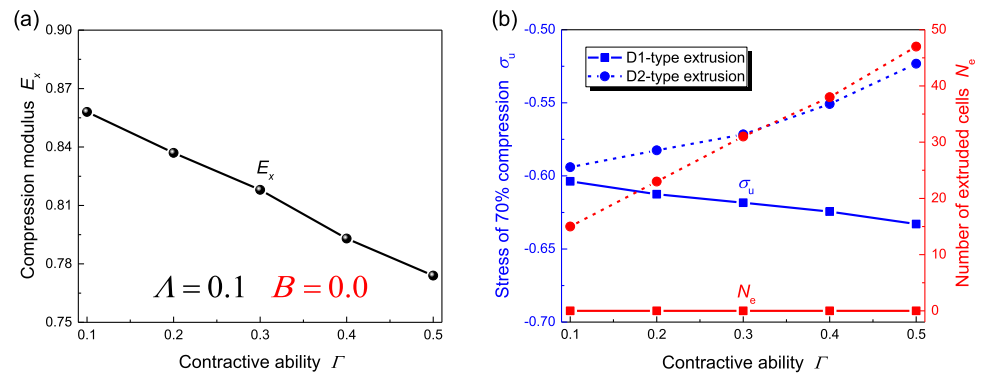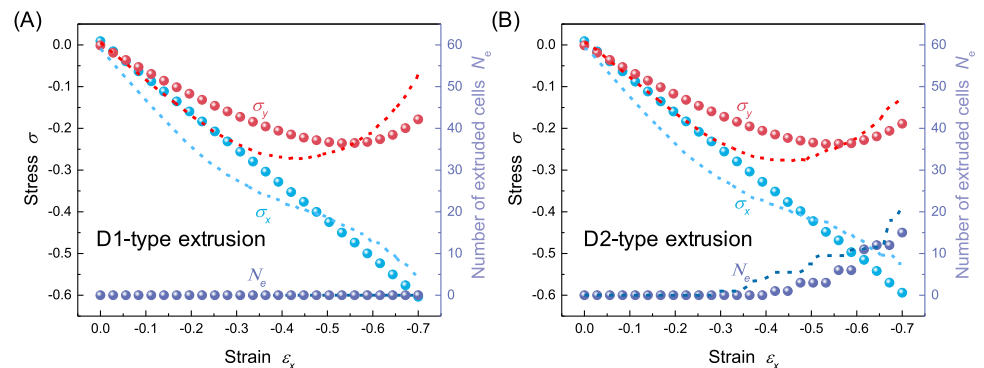

Fig. 8 Mechanical responses of monolayers without microtubules for (**a**) D1-type and (**b**) D2-type cell extrusions under linear strain compression. The dashed lines in the figures are examples of mechanical responses for crowded cell monolayers with microtubules

biological tissues. Future research may thus be directed towards expanding this method to explore and reveal the underlying mechanisms of 3D tissue morphogenesis.

Author contributions

LQD designed the research. QG and LQD performed the research. QG, LQD, and JH analyzed the data and wrote the article.

Data availability No Data associated in the manuscript.

Declarations

Conflict of interest The authors declare that there are no conflicts of interest associated with the present study.

References

1. T. Brunet, A. Bouclet, P. Ahmadi, D. Mitrossilis, B. Driquez, A.-C. Brunet, L. Henry, F. Serman, G. Bealle, C. Menager, F. Dumas-Bouchiat, D. Givord, C. Yanicostas, D. Le-Roy, N.M. Dempsey, A. Plessis, E. Farge, Nat. Commun. **4**, 2821 (2013)
2. C. Guillot, T. Lecuit, Science **340**(6137), 1185 (2013)
3. A. Brugues, E. Anon, V. Conte, J.H. Veldhuis, M. Gupta, J. Colombelli, J.J. Munoz, G.W. Brodland, B. Ladoux, X. Trepat, Nat. Phys. **10**(9), 684 (2014)
4. Y.C. Wang, Z. Khan, M. Kaschube, E.F. Wieschaus, Nature **484**(7394), 390 (2012)
5. G.K. Xu, Y. Liu, Z.L. Zheng, J. Biomech. **49**(3), 401 (2016)
6. K.C. Hart, J. Tan, K.A. Siemers, J.Y. Sim, B.L. Pruitt, W.J. Nelson, M. Gloerich, Proc. Natl. Acad. Sci. U. S. A. **114**(29), E5845 (2017)
7. P. Friedl, D. Gilmour, Nat. Rev. Mol. Cell Bio. **10**(7), 445 (2009)
8. L. Ding, M.J. Ellis, S. Li, D.E. Larson, K. Chen, J. Wallis, C.C. Harris, M.D. McLellan, R.S. Fulton, L.L. Fulton, R.M. Abbott, J. Hoog, D.J. Dooling, D.C. Koboldt, H. Schmidt, J. Kalicki, Q. Zhang, L. Chen, L. Lin, M.C. Wendl, J.F. McMichael, V.J. Magrini, L. Cook, S.D. McGrath, T.L. Vickery, E. Appelbaum, K. DeSchryver,

Eur. Phys. J. Spec. Top. (2023) 232:2717–2725

2725

S. Davies, T. Guintoli, L. Lin, R. Crowder, Y. Tao, J.E. Snider, S.M. Smith, A.F. Dukes, G.E. Sanderson, C.S. Pohl, K.D. Delehaunty, C.C. Fronick, K.A. Pape, J.S. Reed, J.S. Robinson, J.S. Hodges, W. Schierding, N.D. Dees, D. Shen, D.P. Locke, M.E. Wiechert, J.M. Eldred, J.B. Peck, B.J. Oberkfell, J.T. Lolofie, F. Du, A.E. Hawkins, M.D. O'Laughlin, K.E. Bernard, M. Cunningham, G. Elliott, M.D. Mason, D.M. Thompson Jr., J.L. Ivanovich, P.J. Goodfellow, C.M. Perou, G.M. Weinstock, R. Aft, M. Watson, T.J. Ley, R.K. Wilson, E.R. Mardis, Nature **464**(7291), 999 (2010)

9. X. Serra-Picamal, V. Conte, R. Vincent, E. Anon, D.T. Tambe, E. Bazellieres, J.P. Butler, J.J. Fredberg, X. Trepat, Nat. Phys. **8**(8), 628 (2012)

10. X. Trepat, M.R. Wasserman, T.E. Angelini, E. Millet, D.A. Weitz, J.P. Butler, J.J. Fredberg, Nat. Phys. **5**(6), 426 (2009)

11. A. Puliafito, L. Hufnagel, P. Neveu, S. Streichan, A. Sigal, D.K. Fygenson, B.I. Shraiman, Proc. Natl. Acad. Sci. U. S. A. **109**(3), 739 (2012)

12. P. Campinho, M. Behrndt, J. Ranft, T. Risler, N. Minc, C.-P. Heisenberg, Nat. Cell Biol. **15**(12), 1405 (2013)

13. A.R. Harris, L. Peter, J. Bellis, B. Baum, A.J. Kabla, G.T. Charras, Proc. Natl. Acad. Sci. U. S. A. **109**(41), 16449 (2012)

14. A.R. Harris, A. Daeden, G.T. Charras, J. Cell Sci. **127**(11), 2507 (2014)

15. G.T. Eisenhoffer, P.D. Loftus, M. Yoshigi, H. Otsuna, C.-B. Chien, P.A. Morcos, J. Rosenblatt, Nature **484**(7395), 546 (2012)

16. E. Marinari, A. Mehonic, S. Curran, J. Gale, T. Duke, B. Baum, Nature **484**(7395), 542 (2012)

17. Y. Liu, G.K. Xu, L.Y. Zhang, H.J. Gao, Soft Matter **15**(42), 8441 (2019)

18. G.A. Reddy, P. Katira, Soft Matter **18**(19), 3713 (2022)

19. D. Bi, J.H. Lopez, J.M. Schwarz, M.L. Manning, Nat. Phys. **11**(12), 1074 (2015)

20. D.B. Staple, R. Farhadifar, J.C. Roeper, B. Aigouy, S. Eaton, F. Juelicher, Eur. Phys. J. E **33**(2), 117 (2010)

21. J. Ranft, M. Basan, J. Elgeti, J.-F. Joanny, J. Prost, F. Juelicher, Proc. Natl. Acad. Sci. U. S. A. **107**(49), 20863 (2010)

22. Z.Y. Liu, B. Li, Z.L. Zhao, G.K. Xu, X.Q. Feng, H.J. Gao, Phys. Rev. E **102**(1), 012405 (2020)

23. A.G. Fletcher, M. Osterfield, R.E. Baker, S.Y. Shvartsman, Biophys. J. **106**(11), 2291 (2014)

24. S.Z. Lin, S. Ye, G.K. Xu, B. Li, X.Q. Feng, Biophys. J. **115**(9), 1826 (2018)

25. A.G. Fletcher, F. Cooper, R.E. Baker, Philos. Trans. R. Soc. B **372**(1720), 20150519 (2017)

26. C.S. Chen, M. Mrksich, S. Huang, G.M. Whitesides, D.E. Ingber, Science **276**(5317), 1425 (1997)

27. S.A. Gudipaty, J. Lindblom, P.D. Loftus, M.J. Redd, K. Edes, C.F. Davey, V. Krishnegowda, J. Rosenblatt, Nature **543**(7643), 118 (2017)

28. M. Basan, J. Elgeti, E. Hannezo, W.-J. Rappel, H. Levine, Proc. Natl. Acad. Sci. U. S. A. **110**(7), 2452 (2013)

29. N. Sepulveda, L. Petitjean, O. Cochet, E. Grasland-Mongrain, P. Silberzan, V. Hakim, PLoS Comput. Biol. **9**(3), e1002944 (2013)

30. F. Graner, J.A. Glazier, Phys. Rev. Lett. **69**(13), 2013 (1992)

31. M. Chiang, D. Marenduzzo, Europhys. Lett. **116**(2), 28009 (2016)

32. X. Yin, B.C. Wang, L. Lei, L.Y. Zhang, G.K. Xu, J. Mech. Phys. Solids **169**, 105077 (2022)

33. L.Y. Zhang, Y. Li, G.K. Xu, X.Q. Feng, Proc. R. Soc. A-Math. Phys. Eng. Sci. **475**(2228), 20180812 (2019)

34. X. Yin, Y. Li, L.Y. Zhang, G.K. Xu, Compos. Struct. **234**, 111693 (2020)

35. L.Y. Zhang, X. Yin, J. Yang, A. Li, G.K. Xu, Compos. Sci. Technol. **207**, 108740 (2021)

36. L.Y. Zhang, H.P. Zhao, X.Q. Feng, Arch. Appl. Mech. **85**(3), 383 (2015)

37. Y. Liu, J. Cheng, H. Yang, G.-K. Xu, Appl. Phys. Lett. **117**, 21 (2020)

38. Y. Qin, Y.H. Li, L.Y. Zhang, G.K. Xu, J. Mech. Phys. Solids **137**, 103872 (2020)

39. Y. Liu, L.Y. Zhang, B.C. Wang, G.K. Xu, X.Q. Feng, J. Mech. Phys. Solids **147**, 104280 (2021)

40. S.Z. Lin, B. Li, X.Q. Feng, Acta Mech. Sin. **33**(2), 250 (2017)

41. L.Y. Zhang, Y. Li, Y.P. Cao, X.Q. Feng, Eng. Struct. **58**, 36 (2014)

42. L.Y. Zhang, Y. Li, Y.P. Cao, X.Q. Feng, H.J. Gao, J. Appl. Mech. Trans. ASME **80**(6), 061018 (2013)

43. R. Farhadifar, J.C. Roper, B. Algouy, S. Eaton, F. Julicher, Curr. Biol. **17**(24), 2095 (2007)

44. A. Tzur, R. Kafri, V.S. LeBleu, G. Lahav, M.W. Kirschner, Science **325**(5937), 167 (2009)

45. R. Levayer, C. Dupont, E. Moreno, Curr. Biol. **26**(5), 670 (2016)

46. G.K. Xu, Y. Liu, B. Li, Soft Matter **11**(45), 8782 (2015)

47. A.R. Harris, J. Bellis, N. Khalilgharibi, T. Wyatt, B. Baum, A.J. Kabla, G.T. Charras, Nat. Protoc. **8**(12), 2516 (2013)